

# ON THE NATURE OF EXTREMELY RED OBJECTS: THE 2 Ms CHANDRA DEEP FIELD-NORTH SURVEY RESULTS

C. VIGNALI, D. M. ALEXANDER, F. E. BAUER, W. N. BRANDT,

A. E. HORNSCHEMEIER, G. P. GARMIRE, D. P. SCHNEIDER

*Department of Astronomy & Astrophysics, The Pennsylvania State University,  
525 Davey Laboratory, University Park, PA 16802, USA*

*E-mail: chris, davo, fbauer, niel, annh, garmire, and dps@astro.psu.edu*

Understanding the nature of Extremely Red Objects [EROs;  $(I - K) \geq 4$ ] is one of the most challenging issues in observational cosmology. Here we report on the X-ray constraints provided by the 2 Ms *Chandra* Deep Field-North Survey (CDF-N). X-ray emission has been detected from 11 out of 36 EROs ( $\approx 30\%$ ). Five of these have hard X-ray emission and appear to be obscured AGNs, while non-AGN emission (star formation or normal elliptical galaxy emission) is likely to be the dominant source of X-rays from the soft X-ray sources detected at the faintest X-ray flux levels.

## 1 Introduction

EROs were serendipitously discovered more than a decade ago<sup>1</sup> and have optical/near-IR colors consistent with those expected for passively evolving elliptical galaxies and dust-enshrouded star-forming galaxies<sup>2</sup> at  $z \gtrsim 1$ . Evidence for elliptical galaxies within the ERO population has been found from optical spectroscopic and morphological studies,<sup>3,4</sup> while submm-IR observations have provided clear examples of dust-enshrouded galaxies.<sup>5,6</sup> However, until recently the fraction of the ERO population hosting AGNs was unknown. Arguably, the clearest evidence for AGN activity is found from X-ray observations.<sup>7</sup> Here we provide an update on the 1 Ms CDF-N results<sup>8</sup> using the 2 Ms *Chandra* exposure, yielding the tightest X-ray constraints on the ERO population to date.

## 2 The samples

The 2 Ms CDF-N is comprised of 20 observations taken over 27 months and reaches an on-axis 0.5–2 keV (2–8 keV) flux limit of  $\approx 1.5 \times 10^{-17}$  erg cm<sup>-2</sup> s<sup>-1</sup> ( $\approx 1 \times 10^{-16}$  erg cm<sup>-2</sup> s<sup>-1</sup>).<sup>9</sup> The region investigated in this study covers  $8.4' \times 8.4'$  centered on the Hubble Deep Field-North (HDF-N). Two samples are defined in this study: 1) Moderate-depth sample [ $K < 20.1$ ], including 29 EROs (10 with X-ray detections;  $\approx 34\%$ ); 2) Deep Sample [ $K < 22$ ], comprising 9 EROs in the HDF-N only (3 with X-ray detections;  $\approx 33\%$ ), 2 of these EROs are in common with the moderate-depth sample. Seven EROs are detected in X-rays by WAVDETECT using a false-positive probability threshold of  $10^{-7}$ ; for

the others, thresholds of  $10^{-5}$  (2 EROs) and  $10^{-4}$  (2 EROs) were adopted.

### 3 Colors and morphologies of X-ray detected EROs

The  $V - I$  versus  $I - K$  colors of all EROs are shown in Fig. 1. The overall colors of EROs are consistent with those of  $z \approx 1$ –2 early-type spiral and elliptical galaxies. The X-ray detected EROs (filled circles) have the same spread in

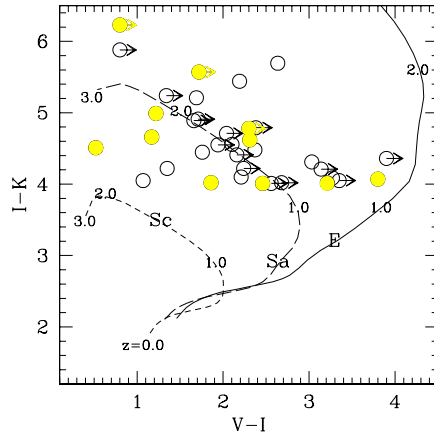


Figure 1:  $V - I$  vs.  $I - K$  colors for all of the EROs in the two samples. The filled circles indicate the X-ray detected EROs. Note that the galaxy tracks shown do not include evolutionary effects and consequently present redder  $V - I$  colors than those expected.

colors as the X-ray undetected ones, suggesting that the X-ray emission is not dependent on the host galaxy type. Two examples of X-ray detected EROs in the HDF-N are shown in Fig. 2, demonstrating the diversity of the ERO population. In the left panel the ERO (the left-most galaxy) is a  $z=1.52$  emission-line galaxy with a spiral/disturbed morphology, while in the right panel the ERO (at  $z=1.32$  photometric) has an elliptical morphology.

### 4 X-ray constraints on the nature of EROs

The effective X-ray photon index ( $\Gamma$ ) of a source can provide a basic constraint on its nature (see Fig. 3). Obscured AGNs have considerably flatter  $\Gamma$  than the canonical  $\Gamma \approx 2.0$  photon index of unobscured AGNs<sup>10</sup> due to photo-electric absorption of the X-ray emission, and they often have X-ray luminosities larger than  $10^{42}$  erg s<sup>-1</sup>. On the other hand, star-forming galaxies often have X-ray emission consistent with that of  $\Gamma \approx 2.0$  power-law emission,<sup>11</sup> and very few starburst galaxies have X-ray luminosities in excess of  $\approx 10^{42}$  erg s<sup>-1</sup>. Passive ellipticals have often X-ray emission consistent with  $\Gamma=1.6$ –1.8 and X-ray

luminosities,  $\lesssim 10^{41}$  erg s $^{-1}$  $^{12}$ . The X-ray detected EROs with  $\Gamma < 1.0$  are likely to host obscured AGNs, and their X-ray luminosities (few  $\times 10^{42}$  erg s $^{-1}$  at  $z=1$ ) agree with this interpretation. Also, the X-ray brightest ERO is likely to be an AGN based on its X-ray luminosity ( $\approx 10^{43}$  erg s $^{-1}$  at  $z=1$ ). Therefore at least 5 of the X-ray detected EROs are likely to host AGNs ( $\approx 50\%$  of the X-ray detected EROs and  $\approx 14\%$  of the ERO population). The average stacked X-ray spectral slope of the other 4 EROs with X-ray constraints ( $\Gamma > 1.0$ ), their X-ray luminosities ( $< 10^{42}$  erg s $^{-1}$  at  $z=1$ ), and multi-wavelength constraints suggest that they could be starburst galaxies<sup>8</sup> or low-luminosity AGNs. Some of these sources also tend to have irregular optical morphologies and extremely red colors [i.e.,  $(I - K) > 5$ ]. Stacking analysis of the X-ray undetected EROs provides an X-ray detection in the 0.5–2 keV band (open circle in Fig. 3) consistent with emission from  $L_\star$  elliptical galaxies. Further constraints on the nature of X-ray detected EROs come from X-ray spectral analysis of the four EROs with more than 80 counts (see Fig. 4 for one example). When modeled with  $\Gamma = 2$  power laws (using the Cash statistic), all four appear to be absorbed by column densities of  $N_H \approx (0.1 - 2.0) \times 10^{23}$  cm $^{-2}$  (at  $z=1$ ). There is no strong evidence for iron K $\alpha$  emission lines.

## References

- [1] R. Elston, G.H. Rieke and M.J. Rieke, *Astrophys. J.* **331**, L77 (1988).
- [2] L. Pozzetti and F. Mannucci, *Mon. Not. R. Astr. Soc.* **317**, L17 (2000).
- [3] A. Cimatti *et al.*, *Astron. Astrophys.* **381**, L68 (2002).
- [4] G. Moriondo, A. Cimatti and E. Daddi, *Astron. Astrophys.* **364**, 26 (2000).
- [5] A. Cimatti, P. Andreani, H. Rottgerring and R. Tilanus, *Nature* **392**, 895 (1998).
- [6] J. Afonso, B. Mobasher, B. Chan and L. Cram, *Astrophys. J.* **559**, L101 (2001).
- [7] A.E. Hornschemeier *et al.*, *Astrophys. J.* **554**, 742 (2001).
- [8] D.M. Alexander *et al.*, *Astron. J.* **123**, 1149 (2002).
- [9] D.M. Alexander *et al.*, in preparation (2003).
- [10] I.M. George *et al.*, *Astrophys. J.* **531**, 52 (2000).
- [11] D.-W Kim, G. Fabbiano and G. Trinchieri, *Astrophys. J. Suppl.* **80**, 645 (1992).
- [12] S. Pellegrini, *Astron. Astrophys.* **351**, 487 (1999).

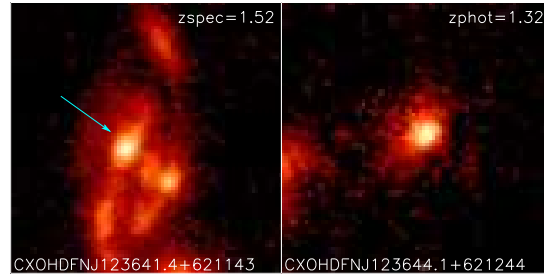


Figure 2: Two examples of X-ray detected EROs in the HDF-N (*HST F814W*-filter images).

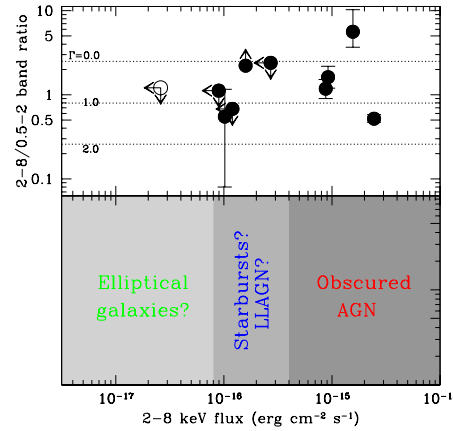


Figure 3: Band ratios (i.e., the ratio of the 2–8 keV to 0.5–2 keV count rates) vs. 2–8 keV fluxes for the 9 EROs with X-ray constraints (filled circles). The open circle shows the stacking analysis result for the X-ray undetected EROs. Effective  $\Gamma$  are also indicated.

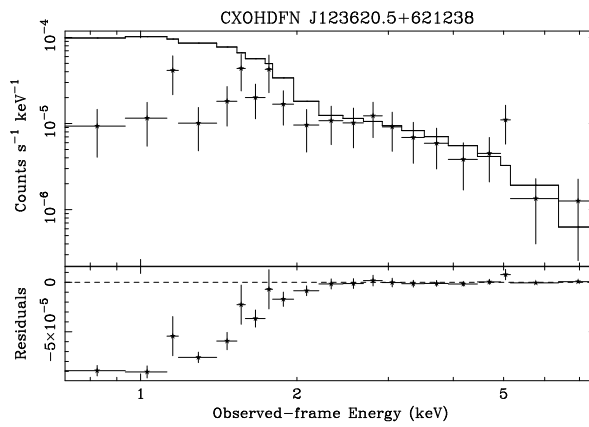


Figure 4: CXO HDFN J123620.5+621238 (binned to 5 counts/bin for presentation purposes) fitted with an unabsorbed  $\Gamma=2$  power law. A deficit of counts below 2 keV is clearly present. This source has  $\approx 110$  counts in the 0.5–8 keV band.